

Comprehensive optical characterization of atomically thin NbSe₂Heather M. Hill,¹ Albert F. Rigosi,^{1,*} Sergiy Krylyuk,^{2,3} Jifa Tian,^{1,4} Nhan V. Nguyen,¹ Albert V. Davydov,²
David B. Newell,¹ and Angela R. Hight Walker¹¹Physical Measurement Laboratory, National Institute of Standards and Technology, Gaithersburg, Maryland 20899, USA²Material Measurement Laboratory, National Institute of Standards and Technology, Gaithersburg, Maryland 20899, USA³Theiss Research, Inc., La Jolla, California 92037, USA⁴Department of Physics and Astronomy, and Birk Nanotechnology Center, Purdue University, West Lafayette, Indiana 47907, USA

(Received 10 August 2018; revised manuscript received 19 September 2018; published xxxxxx)

Transition-metal dichalcogenides (TMDCs) have offered experimental access to quantum confinement in one dimension. In recent years, metallic TMDCs like NbSe₂ have taken center stage with many of them exhibiting interesting temperature-dependent properties such as charge density waves and superconductivity. In this paper, we perform a comprehensive optical analysis of NbSe₂ by utilizing Raman spectroscopy, differential reflectance contrast, and spectroscopic ellipsometry. These analyses, when coupled with Kramers-Kronig analysis, allow us to extract the dielectric functions of bulk and atomically thin NbSe₂ and relate them to the resonant behavior of the Raman spectra.

DOI: [10.1103/PhysRevB.00.005100](https://doi.org/10.1103/PhysRevB.00.005100)

I. INTRODUCTION

Transition-metal dichalcogenides (TMDCs) are a class of materials, which when reduced to two dimensions yield many fascinating properties, including, but not limited to, the exhibition of a direct band gap [1–7] and distinct many-body effects [8–10]. Moreover, these materials have extensive applicability in the advancement of optoelectronics, photovoltaics, spintronics, energy storage, and biophysical systems [11–14]. Metallic TMDCs, such as NbSe₂, exhibit properties such as the charge density wave states [15–22], superconductivity [23–27], and other quantum phenomena that persist in the monolayer limit [28–31]. NbSe₂ has been studied by various nonoptical methods [32–36], as well as optical ones in the case of bulk NbSe₂ [37]. While there have been a number of optical investigations of bulk NbSe₂ for obtaining Raman spectra [38] and optical constants [39,40], there are few works that provide a more comprehensive review of the optical properties as the thickness is decreased to a monolayer [41–45]. Furthermore, research on the dielectric function of atomically thin NbSe₂ is limited [46].

In this paper, detailed optical spectroscopies were utilized to complete a thorough examination of atomically thin flakes exfoliated from NbSe₂ crystals grown using the chemical vapor transport (CVT) method. Raman spectra were acquired over a large parameter space, including layer number, excitation wavelength, and temperature. Specifically, flakes were characterized with traditional [47–49] and resonance [50–56] Raman spectroscopy and verified to be superconducting by measuring electrical transport. To further characterize thin NbSe₂ we used differential reflectance contrast (DRC), which reveals both the reflectivity of the material and, when paired with Kramers-Kronig analysis (KKA), the dielectric function

$\varepsilon(E)$ as a function of energy. As an accompanying technique to DRC, spectroscopic ellipsometry (SE) was also used to directly confirm $\varepsilon(E)$ for bulk NbSe₂, substantiating the validity of using KKA to extract the dielectric function of mono- to few-layer NbSe₂ for photon energies in the visible range (between 1.15 eV and 3.5 eV).

II. EXPERIMENTAL METHODS

A. Crystal growth and sample preparation

Centimeter-sized NbSe₂ single crystals were grown using the iodine-assisted CVT method. Polycrystalline NbSe₂ powders were synthesized by reacting stoichiometric amounts of Nb (99.9%, Strem Chemicals) and Se (99.999%, Strem Chemicals) [57] powders in vacuum-sealed quartz ampoule at 850 °C for three days. Next, quartz ampoules containing less than 1.5 g of NbSe₂ charge and less than 80 mg (3.7 mg/cm³) of I₂ transport agent were sealed under vacuum and placed in a single-zone furnace. Temperatures at the charge and growth zones were between 825 °C and 700 °C and the growth duration was 140 h. NbSe₂ crystals were mechanically exfoliated onto silicone elastomer polydimethylsiloxane and then transferred onto both Si/SiO₂ (oxide thickness of 300 nm) and fused quartz substrates.

B. Traditional and resonance Raman spectroscopy

Traditional and resonance Raman spectroscopy was performed on bulk (approximately 50 nm) and thin (four layers or fewer) NbSe₂ in an inert gas environment as a function of temperature, excitation wavelength, and polarization. For the latter, the polarization of the incoming light was kept fixed while the parallel and cross components of the response were measured separately. The flake thickness was verified using the energy of the Raman shear mode and E_{2g} mode [21,43]. Raman spectra were collected by a Horiba T64000 triple-

*albert.rigosi@nist.gov

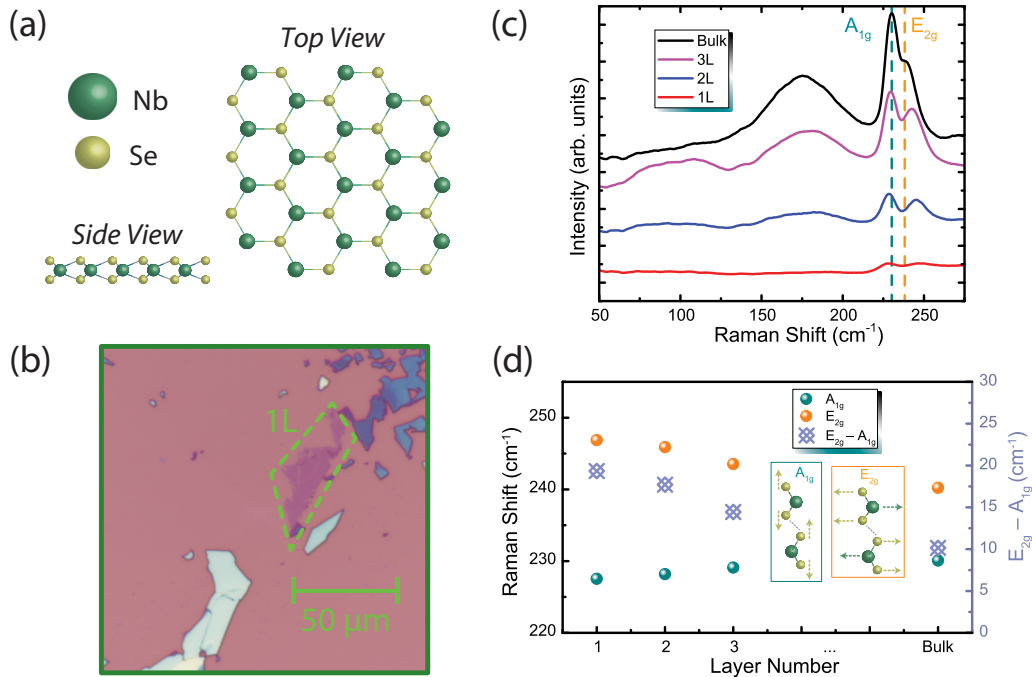


FIG. 1. (a) An illustration of the crystal structure of monolayer 2H-NbSe₂, along with (b) an optical image of an example flake mechanically exfoliated onto Si/SiO₂. The area containing the monolayer (1L) flake is enclosed by a dashed green line. (c) Raman results for 1L, 2L, 3L, and bulk NbSe₂ for an excitation wavelength of 514 nm. The dashed dark cyan and orange lines are meant to guide the eye to the bulk A_{1g} and E_{2g} modes, respectively. (d) The positions of the A_{1g} and E_{2g} modes are plotted as a function of layer number (left vertical axis) with dark cyan and orange points, respectively. The separation of the two modes (labeled on the right vertical axis) is shown with a set of crosses. The insets are visualizations of the mode vibrations.

83 grating spectrometer [57] and measured at temperatures from
 84 300 K to 4 K. Discrete excitation lines from the following
 85 lasers—argon ion, helium neon, and tunable dye, including,
 86 but not limited to, 476.2 nm, 632.8 nm, 514 nm, and 570 nm—
 87 were used with powers ranging from 1 μW to 500 μW and
 88 spot sizes of about 1 μm. Acquisition times varied between
 89 10 min and 30 min.

90 C. Differential reflectance contrast spectroscopy

91 Another optical technique used was DRC, which involves
 92 probing a sample of interest by a combined broadband emis-
 93 sion from a halogen lamp with a spot size of approximately
 94 10 μm. The optical responses of mono- to few-layer NbSe₂
 95 were characterized from the DRC spectra, which are la-
 96 beled as $\frac{\Delta R}{R}$. Here, $\frac{\Delta R}{R} = \frac{R_{\text{NbSe}_2} - R_{\text{quartz}}}{R_{\text{quartz}}}$, where R_{NbSe_2} is the
 97 reflectance of the flake on top of the fused quartz substrate,
 98 and R_{quartz} denotes the reflectance of the bare fused quartz
 99 substrate. The reflected light was collected by a spectrometer.
 100 To inhibit the effects of oxidation, flakes were exfoliated
 101 and immediately measured in ambient conditions at room
 102 temperature over a wavelength range of 350 nm to 1080 nm
 103 (photon energies of 1.15 eV–3.5 eV) with 0.75-nm resolution.

104 D. Spectroscopic ellipsometry

105 SE measurements were performed with a Woollam M-
 106 2000 ellipsometer [57] covering a wavelength range from
 107 about 145 nm to 1240 nm (1.24 eV to 5.88 eV) with 1.25-nm
 108 resolution. The elliptical spot size measured approximately

109 100 μm along the semiminor axis and 200 μm to 300 μm
 110 along the semimajor axis. SE is a measurement of the change
 111 in phase and polarization state of the light reflected from
 112 NbSe₂. Only bulk material was used to directly extract $\varepsilon(E)$.
 113 Data were acquired at two angles of incidence (60° and 70°)
 114 and were converted by the software from Fresnel reflection
 115 coefficients representative of *p* and *s* polarized light (R_p and
 116 R_s) to the related quantities Ψ and Δ , where $\frac{R_p}{R_s} = e^{i\Delta} \tan \Psi$.
 117 The dielectric function of the NbSe₂ was then converted from
 118 Ψ and Δ directly. The advantage of SE is that it can be
 119 used to complement DRC measurements for verifying a ma-
 120 terial's dielectric behavior by using the WVASE32 modeling
 121 program [57].

122 III. RAMAN CHARACTERIZATION OF 123 SUPERCONDUCTING NIOBIUM DISELENIDE

124 Figure 1(a) shows an illustration of the crystal structure of
 125 monolayer 2H-NbSe₂, with an accompanying optical image
 126 shown in Fig. 1(b). The Raman spectra of the A_{1g} and E_{2g}
 127 modes for the CVT-grown crystal, taken with a 514-nm laser,
 128 are summarized in Fig. 1(c) for bulk, trilayer (3L), bilayer
 129 (2L), and monolayer (1L) NbSe₂. The soft Raman mode, or
 130 the second-order scattering process of two phonons, is also
 131 shown. In all spectra, the A_{1g}, E_{2g}, and soft Raman modes
 132 were fit with Lorentzian peaks to extract the Raman shift, full
 133 width at half maximum (FWHM), and integrated intensity.
 134 The bulk A_{1g}, E_{2g}, and soft modes are centered approximately
 135 at 230 cm⁻¹, 240 cm⁻¹, and 180 cm⁻¹, respectively, and in
 136 agreement with the literature [21,46,55,58]. The A_{1g} and

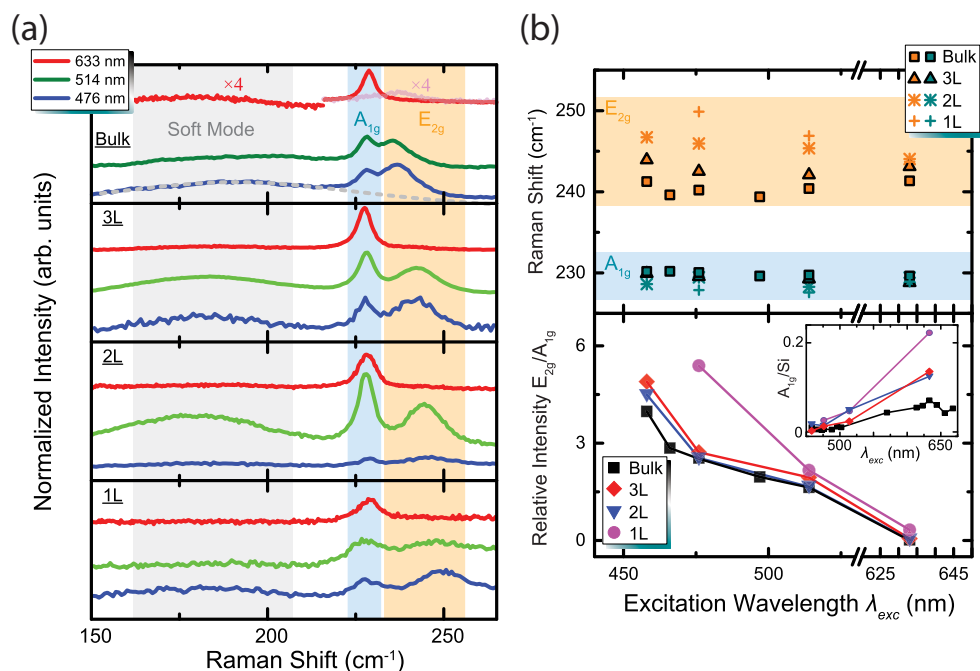


FIG. 2. (a) Raman spectra are acquired for several wavelengths for 1L, 2L, 3L, and bulk NbSe₂. The gray, blue, and orange bands highlight regions where the soft mode, A_{1g}, and E_{2g} modes are observed, respectively. For the case of bulk, the soft mode and the E_{2g} mode are amplified by a factor of 4 for clarity in the 633-nm spectrum. (b) The resonance Raman data are summarized by their peak positions in the top panel, with the blue and orange bands still indicating the A_{1g} and E_{2g} modes, respectively. The bottom panel shows the relative intensities of E_{2g} and A_{1g}, with the inset showing the relative intensity of A_{1g} with respect to the silicon peak as measured through the oxide layer.

E_{2g} modes diverge in Fig. 1(d), with the E_{2g} shifting more strongly, as the layer number is reduced to 1L [43].

To further explore the Raman behavior of NbSe₂, spectra were measured as a function of excitation wavelength for cross and parallel polarizations (see the Supplemental Material [59]). The frequency, FWHM, and relative intensities of the Raman peaks were monitored as the laser was changed. All flake thicknesses were measured at three wavelengths or more (with 476 nm, 514 nm, and 633 nm) with bulk being measured at additional wavelengths.

Figure 2(a) shows the Raman spectra obtained with three wavelengths and for varying flake thickness. Three regions of interest are highlighted using gray, blue, and orange bands for the soft, A_{1g}, and E_{2g} modes, respectively. An example of soft mode fitting is shown in the bulk case at 476 nm. For the 633-nm spectrum, both the soft mode and the E_{2g} mode are multiplied by a factor of 4 for clarity. In cross polarized measurements, the A_{1g} mode is not observed, allowing the E_{2g} mode to be readily observed even when its intensity is weak. More details on the soft mode are provided in the Supplemental Material [59].

To better view the overall behavior of the A_{1g} and E_{2g} modes, both their peak positions and relative intensities are shown as a function of wavelength in Fig. 2(b). The same blue and orange bands are used to highlight the modes' behavior with layer number and wavelength. With the resonance Raman data in Fig. 2(b), we find that the E_{2g} Raman mode has a significantly higher intensity relative to A_{1g} when excited with shorter wavelengths and that A_{1g} has increasing relative intensity with longer wavelengths,

which does not align with the scaling of the Raman-scattering strength with wavelength (λ^{-4}). One possible reason for this phenomenon will be addressed at the end of the next section.

Next, temperature-dependent Raman measurements were performed on bulk NbSe₂ as well as resonance measurements performed at 4 K. Figure 3(a) shows the resonance Raman data taken at 4 K, which yields the same relative intensity trends as the room-temperature data. Representative temperature-dependent spectra are shown in Fig. 3(b) at an excitation wavelength of 514 nm. The full temperature-dependent data are summarized in Fig. 3(c) and include the Raman shift, FWHM, and normalized intensity for two wavelengths. When evaluating the behavior of the A_{1g} and E_{2g} modes with decreasing temperature, one can make three observations.

The first trend is an asymptotic redshift of the Raman frequencies with decreasing temperature. The redshift is more pronounced for the E_{2g} mode than the A_{1g} mode, and those same redshifts are larger for 476 nm than for 514 nm. For the FWHM of the modes, only the E_{2g} mode demonstrates significant narrowing with decreasing temperature, while the change in excitation wavelength produces a negligible effect on the width. Lastly, and more importantly, the normalized intensity for both modes generally increases as the temperature decreases. However, the difference in the intensity trend between the two excitation wavelengths is substantial for temperatures above about 30 K with the intensity decreasing much more significantly when excited with 514 nm. One possible reason for this difference could be attributed to the

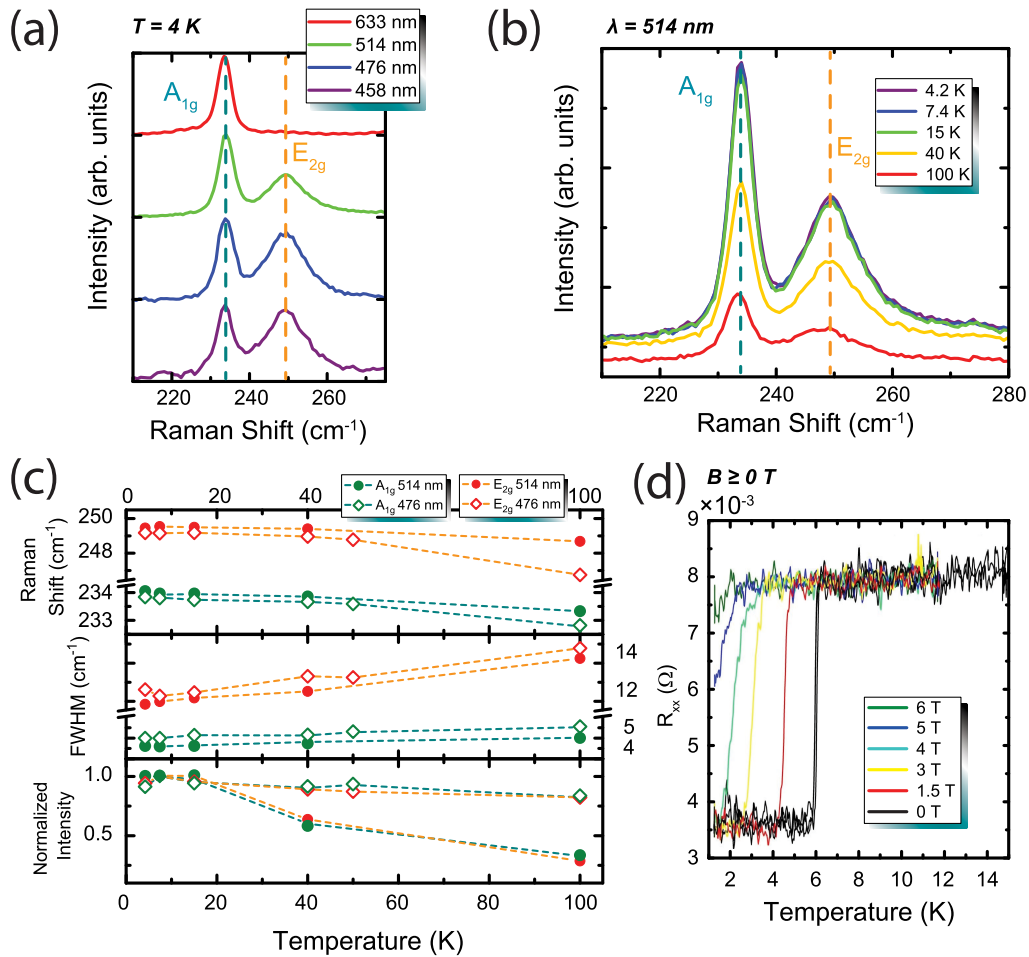


FIG. 3. (a) The Raman spectra of bulk NbSe₂ acquired at 4 K for four different wavelengths. In this figure, all dashed dark cyan and orange lines indicate the A_{1g} and E_{2g} modes, respectively. (b) Raman spectra as a function of temperature for 514-nm excitation. (c) Raman peak positions, FWHMs, and normalized intensities plotted for two wavelengths (indicated by different symbols) as a function of temperature. (d) Resistance of a bulk NbSe₂ device plotted as a function of temperature, with different color curves representing different magnetic field values.

bulk transition at 33 K [47], under which an electron quantum fluid, or charge density wave state, forms.

Finally, we performed temperature-dependent electronic transport measurements, shown in Fig. 3(d). The bulk resistance was measured as a function of temperature with different applied out-of-plane magnetic fields, and, as expected for a superconducting material, a discontinuous drop occurs at the transition temperature of about 6.1 K.

IV. REFLECTANCE ANALYSIS AND THE DIELECTRIC FUNCTION

A. DRC and SE measurements

Additional optical properties can be measured with both SE and DRC, offering a more comprehensive optical description of thin NbSe₂. Figure 4(a) shows the data obtained with DRC. Bulk, 3L, 2L, and 1L flakes were measured on fused quartz to more easily prepare the data for KKA. Specifically, when the thin material is on a transparent substrate, the DRC data are approximately proportional to the absorption (*A*) of the material [60–63]. The absorption is predominantly

determined by the imaginary component of the dielectric function (ϵ_2) and, thus, gives one a starting point to estimate ϵ_2 , with the dielectric function assuming the form $\epsilon(E) = \epsilon_1(E) + i\epsilon_2(E)$. The approximate relation between the DRC and absorption is given in Eq. (1), where n_q is the index of refraction of fused quartz, valued at 1.46:

$$\frac{\Delta R}{R} \approx \frac{4}{n_q^2 - 1} A. \quad (1)$$

The goal is to compare $\epsilon_{\text{bulk}}(E)$ obtained directly with SE to the same quantity obtained using DRC and KKA. A favorable comparison in bulk will support the use of the KKA for determining the dielectric function of mono- to few-layer NbSe₂ where SE measurements are not possible due to sample size. Measurements were done on freshly cleaved bulk material to prevent oxidation effects (see Supplemental Material [59]). The KKA results will be presented in the next subsection. The main benefits of performing SE on a bulk material are twofold: (1) the thickness does not need to be known to within 1 nm since the optical constants do not change with perturbations to bulk thickness, and (2) all incoming light only

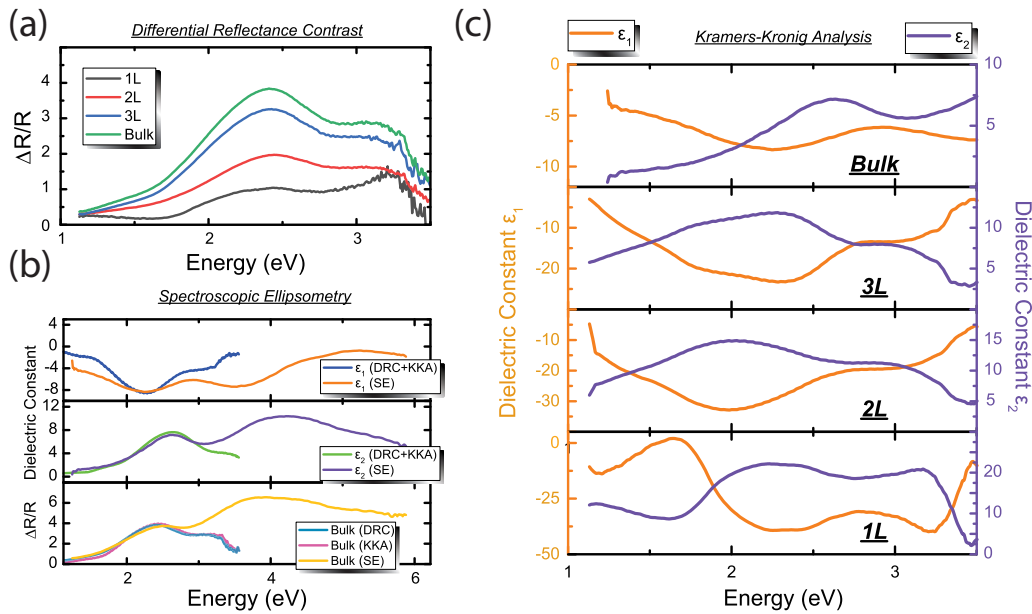


FIG. 4. (a) The DRC spectra for bulk and thin NbSe₂ are shown. These spectra are converted into absorption to obtain an initial guess for ϵ_2 . (b) In the case of bulk NbSe₂, its DRC spectrum is converted and undergoes KKA, with the resulting $\epsilon_{\text{bulk}}(E)$ shown in the top and middle panels as their real (blue) and imaginary (green) components, respectively. This result is compared with the direct measurement of $\epsilon_{\text{bulk}}(E)$ by SE, the real and imaginary components of which are also in the top (orange curve) and middle (purple curve) panels, respectively. The bottom panel shows the original bulk DRC spectrum (light blue), as well as two generated DRC curves. The pink and yellow curves are obtained when regenerating a DRC spectrum with the KKA-extracted and SE-extracted dielectric functions, respectively. (c) The KKA-extracted dielectric functions are shown for bulk, 3L, 2L, and 1L NbSe₂. The real and imaginary components are represented by orange (left vertical axis) and purple (right vertical axis) curves, respectively.

interacts with the bulk. In other cases, light interacting with multiple thin layers having different properties would render the data a representation of a hybrid material. In other words, the so-called pseudodielectric function would be generated, requiring careful layer-by-layer analysis to extract the correct dielectric function for each of the constituent material layers. However, in our case, the output SE data do not hybridize the bulk with the quartz beneath.

When several bulk flakes of NbSe₂ are freshly exfoliated and measured with SE from 1.15 eV to 6.22 eV, we obtain the curves shown in Fig. 4(b). The real component is shown in the top panel as an orange curve and agrees well the KKA counterpart (and will be described in more detail in the next subsection). The same observation holds true for the imaginary component in the middle panel. The dielectric function obtained with SE was then used to calculate an artificial DRC curve to compare with the original data. This comparison is shown in the bottom panel, along with a similarly generated DRC curve from KKA, which will be described later.

B. Kramers-Kronig analysis on DRC data

KKA was used to extract $\epsilon(E)$ for bulk, 3L, 2L, and 1L NbSe₂ from their corresponding DRC measurements [61–64]. As noted before, a rough estimate of the absorption of the material can be calculated from the DRC using Eq. (1). The absorption and ϵ_2 are related by $\frac{\epsilon_2}{A(E)} = \frac{\hbar c}{EL}$, where E is the energy and L is the layer thickness [62]. This estimate provides an initial guess of ϵ_2 which subsequently undergoes

an iterative process to optimize the accuracy of the dielectric function extracted from DRC measurements, the procedure of which is well documented in [63]. This procedure also involves generating a DRC curve using the obtained dielectric function, and only when the generated and experimental DRC curves match to a certain degree of accuracy does one stop the iteration process [63]. With a known ϵ_2 , KKA is performed using Eq. (2):

$$\epsilon_1(E) = 1 + \frac{1}{\pi} \int_{-\infty}^{\infty} \frac{\epsilon_2(E')}{E' - E} dE'. \quad (2)$$

This full procedure is first done for bulk NbSe₂ and yields the result shown in Fig. 4(b). The real (top panel) and imaginary (middle panel) components are presented as blue and green curves, respectively, within the measurement range. The minor disagreement between KKA-obtained $\epsilon_{\text{bulk}}(E)$ and SE-obtained $\epsilon_{\text{bulk}}(E)$ closer to the end points of the DRC energy range is a result of the assumption involved in KKA. It is assumed in Eq. (2) that the optical behavior of the material for all energies is known. However, DRC measurements can only probe the photon energies between 1.15 eV and 3.5 eV. In our calculation, we artificially set the DRC data as approaching zero asymptotically. The expected error from this treatment is underestimating the spectral weight around the end-point regions of ϵ_2 . This underestimation is exactly what happens in the middle panel of Fig. 4(b), where ϵ_2 begins to deviate from SE data after 3 eV.

In the bottom panel of Fig. 4(b), the KKA-obtained $\epsilon_{\text{bulk}}(E)$ is used to generate a DRC curve as a method of

287 verifying the success of the calculation, and the obtained
 288 curve agrees well with the original DRC data. Due to the
 289 limitations of DRC, minor deviations are seen at the end
 290 points with the SE-generated DRC curve in yellow. Overall,
 291 KKA still provides a useful way of extracting $\varepsilon(E)$ over a
 292 range of energies, and, since KKA agrees with a large portion
 293 of the SE-obtained $\varepsilon_{\text{bulk}}(E)$, KKA was utilized to obtain the
 294 dielectric function for the few-layer flakes as well.

295 The DRC curves were used to extract $\varepsilon(E)$ for each
 296 thickness, and the results are shown in Fig. 4(c). For the 1L
 297 case, there is a substantial change in the dielectric function
 298 compared with the gradual changes in thicker flakes' func-
 299 tions, most notably at energies below 2 eV. We attribute the
 300 decrease in the dielectric strength to the reduction of available
 301 electronic states in 1L NbSe₂, which has been previously ex-
 302 plored experimentally and theoretically [44,65]. Specifically,
 303 in 1L, a gap in electronic states was seen along both the Γ -K
 304 and Γ -M directions in the Brillouin zone with angle-resolved
 305 photoemission spectroscopy [44].

306 These functions also reveal some insight onto the observa-
 307 tions made with Raman. Notice that an absorptive response
 308 in the bulk ε_2 is seen at approximately 2.5 eV, and, as the
 309 layer number decreases, the absorption both asymptotically
 310 redshifts to 620 nm (2 eV) and increases in strength. Since ε_2
 311 is the dominant factor in determining the actual absorption
 312 of the material, its behavior as a function of layer number
 313 is crucial in helping us understand the resonance Raman
 314 observations made in Fig. 2(b). For all thicknesses, more light
 315 is absorbed at shorter wavelengths (<500 nm), which may
 316 be the reason for the increased intensity of E_{2g} with shorter
 317 wavelengths. Though this may clarify one of the mechanisms
 318 by which the resonance Raman takes on a local maximum, it

is not fully clear why the A_{1g} intensity increases relative to E_{2g}
 for longer wavelengths when less light is absorbed. This sec-
 ondary phenomenon may require further theoretical analyses.

V. CONCLUSIONS

In summary, we have performed a comprehensive optical
 examination of NbSe₂, both for the bulk crystal and its
 atomically thin layers. The Raman spectra were analyzed
 along with electrical transport to verify the quality of the su-
 perconducting material. Furthermore, the reflectance contrast
 was measured as a function of layer number, allowing for
 the extraction of $\varepsilon(E)$ for bulk, 3L, 2L, and 1L NbSe₂ by
 using Kramers-Kronig analysis. Spectroscopic ellipsometry
 was also performed to further support the accuracy of the
 extracted dielectric functions of NbSe₂.

ACKNOWLEDGMENTS

H.M.H. and A.F.R. would like to thank the National
 Research Council's Research Associateship Program for
 the opportunity. S.K. acknowledges support from the U.S.
 Department of Commerce, **National Institute of Standards
 and Technology** under Financial Assistance Award No.
 70NANB18H155 and would like to thank Theiss Research
 for the opportunity. The authors thank Amber McCreary and
 Thomas Germer for additional assistance.

Attributions. H.M.H. designed the experiment and col-
 lected and analyzed data. A.F.R. provided assistance with
 ellipsometry measurements. S.K. and A.V.D. provided crys-
 tals. J.T. assisted with electrical measurements. The paper was
 written through contributions of all authors.

-
- [1] K. S. Novoselov, D. Jiang, F. Schedin, T. J. Booth, V. V. Khotkevich, S. V. Morozov, and A. K. Geim, *Proc. Natl. Acad. Sci. USA* **102**, 10451 (2005).
- [2] S. Das, J. A. Robinson, M. Dubey, H. Terrones, and M. Terrones, *Annu. Rev. Mater. Sci.* **45**, 1 (2015).
- [3] S. Z. Butler, S. M. Hollen, L. Cao, Y. Cui, J. A. Gupta, H. R. Gutiérrez, T. F. Heinz, S. S. Hong, J. Huang, A. F. Ismach, E. Johnston-Halperin, M. Kuno, V. V. Plashnitsa, R. D. Robinson, R. S. Ruoff, S. Salahuddin, J. Shan, L. Shi, M. G. Spencer, and M. Terrones, *ACS Nano* **7**, 2898 (2013).
- [4] P. Tonndorf, R. Schmidt, P. Böttger, X. Zhang, J. Börner, A. Liebig, M. Albrecht, C. Kloc, O. Gordan, D. R. T. Zahn, S. M. de Vasconcellos, and R. Bratschitsch, *Opt. Express* **21**, 4908 (2013).
- [5] K. F. Mak, C. Lee, J. Hone, J. Shan, and T. F. Heinz, *Phys. Rev. Lett.* **105**, 136805 (2010).
- [6] M. Chhowalla, H. S. Shin, G. Eda, L. J. Li, K. P. Loh, and H. Zhang, *Nat. Chem.* **5**, 263 (2013).
- [7] H. Li, G. Lu, Y. L. Wang, Z. Y. Yin, C. X. Cong, Q. Y. He, L. Wang, F. Ding, T. Yu, and H. Zhang, *Small* **9**, 1974 (2013).
- [8] D. Y. Qiu, F. H. da Jornada, and S. G. Louie, *Phys. Rev. Lett.* **111**, 216805 (2013).
- [9] T. C. Berkelbach, M. S. Hybertsen, and D. R. Reichman, *Phys. Rev. B* **88**, 045318 (2013).
- [10] G. Moody, C. K. Dass, K. Hao, C.-H. Chen, L.-J. Li, A. Singh, K. Tran, G. Clark, X. Xu, G. Berghuser, E. Malic, A. Knorr, and X. Li, *Nat. Commun.* **6**, 8315 (2015).
- [11] Q. Wang, K. Kalantar-Zadeh, A. Kis, J. N. Coleman, and M. S. Strano, *Nat. Nanotechnol.* **7**, 699 (2012).
- [12] S. Manzeli, D. Ovchinnikov, D. Pasquier, O. V. Yazyev, and A. Kis, *Nat. Rev. Mater.* **2**, 17033 (2017).
- [13] G. Wang, A. Chernikov, M. M. Glazov, T. F. Heinz, X. Marie, T. Amand, and B. Urbaszek, *Rev. Mod. Phys.* **90**, 021001 (2018).
- [14] Y.-T. Hsu, A. Vaezi, M. H. Fischer, and E.-A. Kim, *Nat. Commun.* **8**, 14985 (2017).
- [15] D. E. Moncton, J. D. Axe, and F. J. DiSalvo, *Phys. Rev. B* **16**, 801 (1977).
- [16] G. Gruner, *Rev. Mod. Phys.* **60**, 1129 (1988).
- [17] M. D. Johannes and I. I. Mazin, *Phys. Rev. B* **77**, 165135 (2008).
- [18] F. Weber, S. Rosenkranz, J.-P. Castellán, R. Osborn, R. Hott, R. Heid, K.-P. Bohnen, T. Egami, A. H. Said, and D. Reznik, *Phys. Rev. Lett.* **107**, 107403 (2011).
- [19] C. J. Arguello, S. P. Chockalingam, E. P. Rosenthal, L. Zhao, C. Gutierrez, J. H. Kang, W. C. Chung, R. M. Fernandes, S. Jia, A. J. Millis, R. J. Cava, and A. N. Pasupathy, *Phys. Rev. B* **89**, 235115 (2014).
- [20] U. Chatterjee, J. Zhao, M. Iavarone, R. Di Capua, J. P. Castellán, G. Karapetrov, C. D. Malliakas, M. G. Kanatzidis, H. Claus, J. P. C. Ruff, F. Weber, J. vanWezel, J. C. Campuzano, R. Osborn,

- M. Randeria, N. Trivedi, M. R. Norman, and S. Rosenkranz, *Nat. Commun.* **6**, 6313 (2014).
- [21] X. Xi, L. Zhao, Z. Wang, H. Berger, L. Forro, J. Shan, and K. F. Mak, *Nat. Nanotechnol.* **10**, 765 (2015).
- [22] X. Xi, H. Berger, L. Forro, J. Shan, and K. F. Mak, *Phys. Rev. Lett.* **117**, 106801 (2016).
- [23] H. Suderow, V. G. Tissen, J. P. Brison, J. L. Martinez, and S. Vieira, *Phys. Rev. Lett.* **95**, 117006 (2005).
- [24] M. S El-Bana, D. Wolverson, S. Russo, G. Balakrishnan, D. M. Paul, and S. J. Bending, *Supercond. Sci. Technol.* **26**, 125020 (2013).
- [25] N. F. Q. Yuan, K. F. Mak, and K. T. Law, *Phys. Rev. Lett.* **113**, 097001 (2014).
- [26] X. Zhu, Y. Guo, H. Cheng, J. Dai, X. An, J. Zhao, K. Tian, S. Wei, X. C. Zeng, C. Wu, and Y. Xie, *Nat. Commun.* **7**, 11210 (2016).
- [27] C.-S. Lian, C. Si, and W. Duan, *Nano Lett.* **18**, 2924 (2018).
- [28] Y. Zhou, Z. Wang, P. Yang, X. Zu, L. Yang, X. Sun, and F. Gao, *ACS Nano* **6**, 9727 (2012).
- [29] F. Flicker and J. van Wezel, *Nat. Commun.* **6**, 7034 (2015).
- [30] X. Xi, Z. Wang, W. Zhao, J.-H. Park, K. T. Law, H. Berger, L. F., J. Shan, and K. F. Mak, *Nat. Phys.* **12**, 139 (2016).
- [31] L. Bawden, S. P. Cooil, F. Mazzola, J. M. Riley, L. J. Collins-McIntyre, V. Sunko, K. W. B. Hunvik, M. Leandersson, C. M. Polley, T. Balasubramanian, T. K. Kim, M. Hoesch, J. W. Wells, G. Balakrishnan, M. S. Bahramy, and P. D. C. King, *Nat. Commun.* **7**, 11711 (2016).
- [32] J. F. Scott, *Rev. Mod. Phys.* **46**, 83 (1974).
- [33] D. J. Rahn, S. Hellmann, M. Kallane, C. Sohr, T. K. Kim, L. Kipp, and K. Rossnagel, *Phys. Rev. B* **85**, 224532 (2012).
- [34] Y. Noat, J. A. Silva-Guillen, T. Cren, V. Cherkez, C. Brun, S. Pons, F. Debontridder, D. Roditchev, W. Sacks, L. Cario, P. Ordejon, A. Garcia, and E. Canadell, *Phys. Rev. B* **92**, 134510 (2015).
- [35] F. Bischoff, W. Auwärter, J. V. Barth, A. Schiffrin, M. Fuhrer, and B. Weber, *Chem. Mater.* **29**, 9907 (2017).
- [36] C.-Z. Xu, X. Wang, P. Chen, D. Flototto, J. A. Hlevyack, M.-K. Lin, G. Bian, S.-K. Mo, and T.-C. Chiang, *Phys. Rev. Mater.* **2**, 064002 (2018).
- [37] M. A. Measson, Y. Gallais, M. Cazayous, B. Clair, P. Rodiere, L. Cario, and A. Sacuto, *Phys. Rev. B* **89**, 060503(R) (2014).
- [38] A. Mialitsin, *J. Phys. Chem. Solids* **72**, 568 (2011).
- [39] S. V. Dordevic, D. N. Basov, R. C. Dynes, B. Ruzicka, V. Vescoli, L. Degiorgi, H. Berger, R. Gaal, L. Forro, and E. Bucher, *Eur. Phys. J. B* **33**, 15 (2003).
- [40] G. E. Meyers and G. L. Montet, *J. Appl. Phys.* **41**, 4642 (1970).
- [41] Y. Cao, A. Mishchenko, G. L. Yu, E. Khestanova, A. P. Rooney, E. Prestat, A. V. Kretinin, P. Blake, M. B. Shalom, C. Woods, J. Chapman, G. Balakrishnan, I. V. Grigorieva, K. S. Novoselov, B. A. Piot, M. Potemski, K. Watanabe, T. Taniguchi, S. J. Haigh, A. K. Geim, and R. V. Gorbachev, *Nano Lett.* **15**, 4914 (2015).
- [42] A. W. Tsen, B. Hunt, Y. D. Kim, Z. J. Yuan, S. Jia, R. J. Cava, J. Hone, P. Kim, C. R. Dean, and A. N. Pasupathy, *Nat. Phys.* **12**, 208 (2016).
- [43] R. He, J. van Baren, J.-A. Yan, X. Xi, Z. Ye, G. Ye, I.-H. Lu, S. M. Leong, and C. H. Lui, *2D Mater.* **3**, 031008 (2016).
- [44] M. M. Ugeda, A. J. Bradley, Y. Zhang, S. Onishi, Y. Chen, W. Ruan, C. Ojeda-Aristizabal, H. Ryu, M. T. Edmonds, H.-Z. Tsai, A. Riss, S.-K. Mo, D. Lee, A. Zettl, Z. Hussain, Z.-X. Shen, and M. F. Crommie, *Nat. Phys.* **12**, 92 (2016).
- [45] E. Sohn, X. Xi, W.-Y. He, S. Jiang, Z. Wang, K. Kang, J.-H. Park, H. Berger, L. Forro, K. T. Law, J. Shan, and K. F. Mak, *Nat. Mater.* **17**, 504 (2018).
- [46] P. Cudazzo, M. Gatti, and A. Rubio, *New J. Phys.* **15**, 125005 (2013).
- [47] J. C. Tsang, J. E. Smith, Jr., and M. W. Shafer, *Phys. Rev. Lett.* **37**, 1407 (1976).
- [48] Y. Wu, M. An, R. Xiong, J. Shi, and Q. M. Zhang, *J. Phys. D* **41**, 175408 (2008).
- [49] X. Zhang, Q.-H. Tan, J.-B. Wu, W. Shi, and P.-H. Tan, *Nanoscale* **8**, 6435 (2016).
- [50] E. del Corro, H. Terrones, A. Elias, C. Fantini, S. Feng, M. A. Nguyen, T. E. Mallouk, M. Terrones, and M. A. Pimenta, *ACS Nano* **8**, 9629 (2014).
- [51] E. del Corro, A. Botello-Méndez, Y. Gillet, A. L. Elias, H. Terrones, S. Feng, C. Fantini, D. Rhodes, N. Pradhan, L. Balicas, X. Gonze, J.-C. Charlier, M. Terrones, and M. A. Pimenta, *Nano Lett.* **16**, 2363 (2016).
- [52] J. U. Lee, J. Park, Y.-W. Son, and H. Cheong, *Nanoscale* **7**, 3229 (2017).
- [53] M. R. Molas, K. Nogajewski, M. Potemski, and A. Babinski, *Sci. Rep.* **7**, 5036 (2017).
- [54] D. Nam, J.-U. Lee, and H. Cheong, *Sci. Rep.* **5**, 17113 (2015).
- [55] B. R. Carvalho, L. M. Malard, J. M. Alves, C. Fantini, and M. A. Pimenta, *Phys. Rev. Lett.* **114**, 136403 (2015).
- [56] P. Soubelet, A. E. Bruchhausen, A. Fainstein, K. Nogajewski, and C. Faugeras, *Phys. Rev. B* **93**, 155407 (2016).
- [57] Commercial equipment, instruments, and materials are identified in this paper in order to specify the experimental procedure adequately. Such identification is not intended to imply recommendation or endorsement by the National Institute of Standards and Technology or the United States government, nor is it intended to imply that the materials or equipment identified are necessarily the best available for the purpose.
- [58] J. C. Tsang, J. E. Smith, Jr., and M. W. Shafer, *Solid State Commun.* **27**, 145 (1978).
- [59] See Supplemental Material at <http://link.aps.org/supplemental/10.1103/PhysRevB.xx.xxxxxx> for comparisons of the CVT-grown and commercial crystal, soft Raman mode data, polarization-dependent measurements, and details on the oxidation effects on NbSe₂. This material includes Ref. [66].
- [60] A. F. Rigosi, H. M. Hill, Y. L. Li, A. Chernikov, and T. F. Heinz, *Nano Lett.* **15**, 5033 (2015).
- [61] Y. Li, A. Chernikov, X. Zhang, A. Rigosi, H. M. Hill, A. M. van der Zande, D. A. Chenet, E.-M. Shih, J. Hone, and T. F. Heinz, *Phys. Rev. B* **90**, 205422 (2014).
- [62] D. Kecik, C. Bacaksiz, R. T. Senger, and E. Durgun, *Phys. Rev. B* **92**, 165408 (2015).
- [63] H. M. Hill, A. F. Rigosi, S. Chowdhury, Y. Yang, N. V. Nguyen, F. Tavazza, R. E. Elmquist, D. B. Newell, and A. R. Hight Walker, *Phys. Rev. B* **96**, 195437 (2017).
- [64] A. F. Rigosi, H. M. Hill, N. R. Glavin, S. J. Pookpanratana, Y. Yang, A. G. Boosalis, J. Hu, A. Rice, A. A. Allerman, N. Nguyen, C. A. Hacker, R. E. Elmquist, A. R. Hight Walker, and D. B. Newell, *2D Mater.* **5**, 011011 (2018).
- [65] M. Calandra, I. I. Mazin, and F. Mauri, *Phys. Rev. B* **80**, 241108(R) (2009).
- [66] Y. Zhao, Z. Zhang, and Y. Lin, *J. Phys. D* **37**, 3392 (2004).